VSP

Journal of Adhesion Science and Technology 24 (2010) 2511–2529

Journal of ADHESION SCIENCE and TECHNOLOGY
brill.nl/jast

Odd–Even Effects in the Friction of Self-Assembled Monolayers of Phenyl-Terminated Alkanethiols in Contacts of Different Adhesion Strengths

Yutao Yang [a], **Andrew C. Jamison** [b], **David Barriet** [b], **T. Randall Lee** [b] **and Marina Ruths** [a,*]

[a] Department of Chemistry, University of Massachusetts Lowell, 1 University Avenue, Lowell, MA 01854, USA

[b] Department of Chemistry, University of Houston, 4800 Calhoun Road, Houston, TX 77204, USA

Abstract

We have studied the frictional properties of self-assembled monolayers (SAMs) of phenyl-terminated alkanethiols, $C_6H_5(CH_2)_nSH$ ($n = 13$–16) on template-stripped gold. The friction force was measured with atomic force microscopy (AFM), and the magnitude of the adhesion was controlled by immersing the sliding contact in ethanol (giving low adhesion) or dry N_2 gas (giving enhanced adhesion relative to ethanol). We observed a linear friction force as a function of load ($F = \mu L$) in the systems with low adhesion and a non-linear friction force when the adhesion was higher. The non-linear behavior in the adhesive systems appeared to be area-dependent ($F = S_c A$) and was compared to contact areas calculated using the extended Thin-Coating Contact Mechanics (TCCM) model. In ethanol, the coefficient of friction μ was found to be systematically higher for odd values of n (i.e., for the monolayers in which the terminal phenyl group was oriented closer to the surface normal).

Keywords

Phenyl-terminated alkanethiols, self-assembled monolayers (SAMs), friction, adhesion, odd–even, atomic force microscopy (AFM), Thin-Coating Contact Mechanics (TCCM) model

1. Introduction

Self-assembled monolayers (SAMs) are commonly used as model boundary lubricants that reduce friction and protect against wear of surfaces that are in close proximity (in contact or at separations of a few molecular diameters) and at high pressures. Among the properties that affect the frictional response of self-assembled systems are packing density [1–4], molecular chain length [5, 6] and rigidity [7], strength of anchoring to the underlying substrate [8], and end-group functionality

* To whom correspondence should be addressed. Tel.: (978) 934-3692; e-mail: marina_ruths@uml.edu

DOI:10.1163/016942410X508253

[6, 9], all of which have some effect on the lateral cohesion of the monolayer [3, 5, 6, 10, 11] and on the ease with which defects are formed during sliding [1, 3–6].

Monolayers containing aromatic moieties are of interest from a fundamental perspective because of their stronger and more complex intermolecular interactions compared to the better-known alkanethiol and alkylsilane monolayers [10, 11]. Aromatic compounds exhibit potentially useful electronic and optical properties [10], and their stiffness is of practical use for forming end-functionalized monolayers where the orientation of the end-group is unaffected by the gauche defects found in alkane-based systems [10, 11]. The orientation and close-packing in the aromatic systems are affected by the stiffness of the molecules, and it has been shown that even the introduction of a single $–CH_2–$ group between the aromatic moiety and the group anchored to the surface enables a better packing of the resulting monolayer [12, 13], and correspondingly diminished friction [8, 14–16].

The friction of monolayers containing aromatic groups is also of interest from a practical point of view. It is known that nitrogen-, oxygen-, and sulfur-containing aromatic and heteroaromatic molecules contribute to the natural lubricity of mineral-oil-based fuels [17–19], importantly, the hydrogenation process used to lower the aromatic content leads to an increase in friction. Furthermore, biodiesel is commonly blended with standard diesel fuel to improve its properties, and there is also a variety of aromatic and heteroaromatic friction-reducing additives [17–19]. Despite these important applications, there is remarkably limited information available on the molecular-level lubricating properties of aromatic compounds [7, 20]. To this end, we have examined simple aromatic monolayers [8, 14, 15] and a series of polyaromatic thiol-based monolayers [16] that are highly rigid and give a relatively high friction. In this work, we use atomic force microscopy (AFM) to study a series of phenyl-terminated alkanethiol self-assembled monolayers [21] with the same end-group functionality but higher molecular packing than the simple aromatic thiols studied previously.

Friction in single-asperity contacts is commonly observed to depend on the strength of adhesion [8, 16, 22–27], therefore the measurements were done in ethanol, where the adhesion (attraction due to van der Waals forces) is low, and in dry N_2 gas, where the adhesion is higher. As in several of these previous studies [16, 23], we observe here also different functional forms of the friction force F *versus* load (normal force) L in adhesive *versus* non-adhesive systems. In ethanol (low adhesion), the friction force is a linear function of load ($F = \mu L$, where μ is the coefficient of friction), whereas in dry N_2, it shows a non-linear load dependence that is generally associated with a dependence on the contact area ($F = S_c A$, where S_c is the critical shear stress and A the contact area). These non-linear data were compared to contact areas calculated with the extended Thin-Coating Contact Mechanics model recently developed by Reedy [28, 29]. We find an odd–even effect in the coefficient of friction μ as a function of the number of methylene units in the alkane chain, which correlates with the different orientations of the terminal phenyl group of the monolayers.

2. Materials and Methods

2.1. Self-Assembled Monolayers (SAMs)

Phenyl-terminated alkanethiols, $C_6H_5(CH_2)_nSH$, were synthesized as described in Ref. [21], where details on the characterization of the compounds with $n = 13$–15 are given. These adsorbates have been shown to form well-ordered SAMs on gold with a packing density similar to that of *n*-alkanethiols and a herringbone packing of the terminal groups [21]. The analytical data for the new adsorbate ($n = 16$) are provided here.

16-Phenylhexadecanethiol ($C_6H_5(CH_2)_{16}SH$). ^{1}H NMR (300 MHz, $CDCl_3$): δ 7.17–7.28 (m, 5 H), 2.60 (t, $J = 7.8$ Hz, 2 H), 2.52 (q, $J = 7.5$ Hz, 2 H), 1.56–1.63 (m, 4 H), 1.25–1.36 (m, 24 H). ^{13}C NMR (75.6 MHz, $CDCl_3$): δ 143.11, 128.54 (2 C), 128.35 (2 C), 125.68, 36.15, 34.22, 31.68, 29.82 (4 C), 29.79 (2 C), 29.75 (2 C), 29.68, 29.50, 29.24, 28.54, 24.82. Mass: $m/z = 334$ (molecular weight 334.6).

Ellipsometry was used to measure the thickness of the $C_6H_5(CH_2)_{16}SH$ monolayers formed on two slides made from Si(100) wafers, on which 10 nm chromium and 100 nm gold had been deposited. Measurements were done at three distinct points on each slide, and the average value, obtained using a refractive index of 1.45, is given in Table 1. Further technical details and the thicknesses of monolayers with $n = 13$–15 are given in Ref. [21] (cf. Table 1).

For the measurements of friction, SAMs were formed on flat substrates by immersing template-stripped gold on polystyrene backing [14, 30] in 0.4–1 mM solu-

Table 1.
Film thicknesses (T), contact angles (θ) and surface energies (γ_{YD}). Tip radii (R), and coefficients of friction (μ) measured in ethanol

n	T (nm)	θ_{adv} (°)	θ_{rec} (°)	γ_{YD} (mJ/m^2)[b]	Bare Si tip		SAM-covered tip	
					R (nm)	μ[c]	R (nm)	μ[c]
13	2.09[a]	93 ± 2	83 ± 3	35	132	0.25 ± 0.02	66	0.31 ± 0.01
					132	0.26 ± 0.03	88	0.33 ± 0.02
							88	0.30 ± 0.02
14	2.19[a]	92 ± 2	78 ± 2	36	132	0.14 ± 0.01	143	0.21 ± 0.01
					132	0.19 ± 0.01	143	0.23 ± 0.01
15	2.27[a]	93 ± 2	80 ± 2	34	132	0.30 ± 0.01	130	0.38 ± 0.01
					132	0.32 ± 0.01	130	0.42 ± 0.01
					137	0.28 ± 0.02	103	0.37 ± 0.04
					137	0.31 ± 0.06	103	0.34 ± 0.04
16	2.45	94 ± 1	81 ± 2	35	137	0.17 ± 0.01	81	0.32 ± 0.01
					137	0.16 ± 0.01	81	0.29 ± 0.01

[a] Reference [21], $\Delta T = 0.1$ nm.
[b] Equation (1), $\Delta\gamma_{YD} = 1$ mJ/m^2.
[c] Standard deviations from linear fits as in Fig. 2.

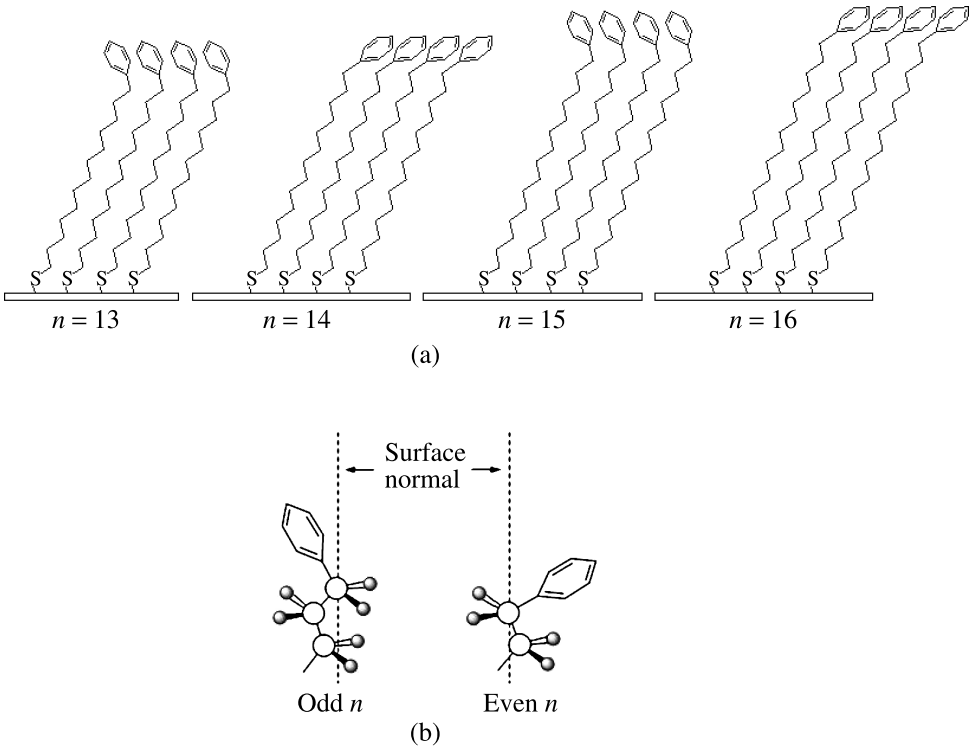

Figure 1. (a) Schematic illustration of the structure of SAMs on gold derived from phenyl-terminated alkanethiols, $C_6H_5(CH_2)_nSH$, $n = 13$–16. (b) Expected orientation of the terminal phenyl group at ca. 30° and 60° from the surface normal for odd and even values of n, respectively.

tion of the thiol in ethanol (Sigma-Aldrich, ⩾99.5%) for 24–48 h. The samples were then removed from the solution, rinsed with ethanol, and blown dry with a stream of dry N_2 gas. The rms roughness of the template-stripped gold was 0.2–0.4 nm, measured over 1 μm^2. Monolayers were also formed on gold-covered AFM tips (see below). Polarization modulation infrared reflection-absorption spectroscopy of phenyl-terminated SAMs on gold has shown that there is a larger chain twist in monolayers with even n [21], and has confirmed the expected orientation of the terminal phenyl group [21, 31]. Schematic drawings of the self-assembled monolayer structures, including the orientation of the terminal phenyl group for odd and even values of n, are shown in Fig. 1.

2.2. Surface and Interfacial Energy

Advancing and receding contact angles of water were measured with a Krüss Drop Shape Analysis System 100. Typical drop volumes were 5–10 μl. The values in Table 1 are averages of 5–8 measurements on different positions on 3–5 different samples and are given with their standard error (standard deviation of the mean). The advancing contact angles agree well with previous data for $n = 13$–15 [21],

where no discernible difference was seen between the different chain lengths. Using the Young–Dupré (YD) equation [32], $W = \gamma_{LV}(1+\cos\theta)$, where γ_{LV} is the surface tension of the liquid, and assuming that the work of adhesion, W, is composed of the dispersion and polar components of the surface energy of the solid and surface tension of the liquid (the Owens–Wendt approach) [33], $W = 2(\sqrt{\gamma_S^d\gamma_L^d} + \sqrt{\gamma_S^p\gamma_L^p})$, then one obtains

$$2\left(\sqrt{\gamma_S^d\gamma_L^d} + \sqrt{\gamma_S^p\gamma_L^p}\right) = \gamma_{LV}(1+\cos\theta). \tag{1}$$

Using equation (1), the surface energy of the solid surface (i.e., the self-assembled monolayer), $\gamma_{YD} = \gamma_S = \gamma_S^d + \gamma_S^p$, can be obtained from the advancing contact angles in Table 1 and Ref. [21] for liquids with different surface tensions $\gamma_{LV} = \gamma_L^d + \gamma_L^p$ (water: $\gamma_L^d = 21.8$ mJ/m^2, $\gamma_L^p = 51$ mJ/m^2; methylene iodide [33]: $\gamma_L^d = 48.5$ mJ/m^2, $\gamma_L^p = 2.3$ mJ/m^2; nitrobenzene [34]: $\gamma_L^d = 38.7$ mJ/m^2, $\gamma_L^p = 5.1$ mJ/m^2). The resulting values of γ_{YD} are listed in Table 1 ($\Delta\gamma_{YD} = 1$ mJ/m^2). In all four SAM systems, the polar contribution to the surface energy of the solid is quite low, $\gamma_S^p \approx 1$ mJ/m^2, i.e., the surface energy of the monolayers arises mainly from dispersion intermolecular interactions.

For comparison with the surface energies from the contact angle measurements and with interfacial energies obtained from our AFM experiments below, values can also be calculated using van der Waals–Lifshitz theory [32]. Some of our measurements of friction were performed by scanning the monolayers with bare (unfunctionalized) Si tips carrying a native oxide layer, and others with monolayer-functionalized gold-covered tips. The van der Waals interactions in the first system were approximated by an asymmetrical three-layer system, $\gamma_{vdW} = A_{132}/(24\pi D_0^2)$, where A_{132} is the Hamaker constant (1 = monolayer, 3 = medium (N_2 or ethanol), 2 = amorphous SiO_2), and $D_0 = 0.165$ nm is the cut-off separation at contact [32]. The interfacial energies in systems with monolayer-functionalized tips were calculated for a symmetrical 5-layer system (gold/monolayer/medium/monolayer/gold, materials 1/2/3/2/1 in equation (2)), as $\gamma_{vdW} = -F_{vdW}(D_0)/(4\pi R)$, where F_{vdW} is the non-retarded van der Waals force between a sphere and a flat surface [32],

$$\frac{F_{vdW}}{R} = -\frac{1}{6}\left(\frac{A_{232}}{D^2} - 2\frac{\sqrt{A_{232}\times A_{121}}}{(D+T)^2} + \frac{A_{121}}{(D+2T)^2}\right), \tag{2}$$

where R is the radius of curvature (AFM tip radius), D is the separation distance (at contact, $D = D_0 = 0.165$ nm), T is the monolayer thickness (Table 1), A_{121} is the Hamaker constant for material 1 interacting across material 2, and A_{232} the Hamaker constant for material 2 interacting across material 3. The Hamaker constants [32] were calculated using a bulk refractive index and dielectric constant of the aromatic compounds estimated from data for compounds with a structure similar to the molecules in our SAMs, 11-phenylheneicosane (1-decylundecylbenzene) [35] and 1-phenylpentadecane [36] (r.i. = 1.48 [35, 36] and $\varepsilon = 2.2$), and bulk

values for N_2 and ethanol. The Hamaker constant for gold interacting across a vacuum or in air ($A = 45.5 \times 10^{-20}$ J) [37] was used in the combining relation [32] $A_{121} = (\sqrt{A_{11}} - \sqrt{A_{22}})^2$. In the asymmetric systems (bare Si tip probing a monolayer), $\gamma_{vdW} = 31$ mJ/m^2 in dry N_2 gas and 2 mJ/m^2 in ethanol. In the symmetric systems (monolayer-covered tip probing monolayer), $\gamma_{vdW} = 32$ mJ/m^2 in N_2 and 3 mJ/m^2 in ethanol.

2.3. Friction Force Microscopy

The friction force, F, was measured over a scan length of 1 μm with atomic force microscopy (AFM) in lateral or friction mode, using a Multimode AFM with Nanoscope IIIa controller (Veeco). Raw data were collected as "friction loops" in Scope mode at different loads (normal force) L, and the measured voltages were converted to force as described in Refs [38] and [39]. The dependence of the friction force on scan rate was found to be weak (in the rate range 0.6–122 μm/s; not shown) and a scan rate of 2 μm/s was chosen for these experiments. The statistical error in F (standard deviation of the mean, from averaging the sliding portion of the friction loop) was ca. 0.2 nN at $F < 50$ nN, and 0.5 nN at higher F, and is not shown in Fig. 2 (and later in Fig. 4) since it is similar to the height of the symbols. The experiments were conducted with bare Si tips (CSC17, MikroMasch) carrying a native silicon oxide layer, and with gold-covered tips (CSC38/Cr-Au) functionalized with phenyl-terminated alkanethiol (the same compound as on the flat substrate). The normal and lateral spring constants of the rectangular cantilevers were determined from their resonance frequency [40, 41] and dimensions measured with scanning electron microscopy (JEOL-7401F), as described previously [16, 38, 39]. In these experiments, the normal spring constants were in the range 0.20–0.55 N/m and the lateral spring constants in the range 25–92 N/m. The tip radii, R, were determined by reverse imaging of a calibration sample (TGT01, MikroMasch) in two orthogonal directions. In this particular batch of tips, $R = 65$–200 nm, which was larger than the manufacturer's specification. This larger radius was advantageous for friction measurements on our self-assembled monolayers, since these typically showed a reversible transition (cf. Results) at pressures of ca. 1 GPa. With smaller tip radii this transition would be reached at very low loads, giving a more limited range of data. The uncertainty in the radius was $\Delta R = 3$ nm ($R < 100$ nm) or 5 nm ($R \geqslant 100$ nm) [16]. Experiments in ethanol were conducted in a fluid cell. For experiments in dry N_2, the AFM was enclosed in a home-made plastic chamber that was continuously purged with a slow stream of N_2 gas (Airgas, 99.5%). The humidity was monitored with a Vaisala DM70 dewpoint meter. A relative humidity of $\leqslant 0.7\%$ was reached after purging for 2 h.

2.4. Contact Mechanics

At low loads, the radius of the contact area between an AFM tip and a monolayer-functionalized substrate can be similar to the thickness of the monolayer. If the elastic modulus of the monolayer is significantly lower than that of the substrates,

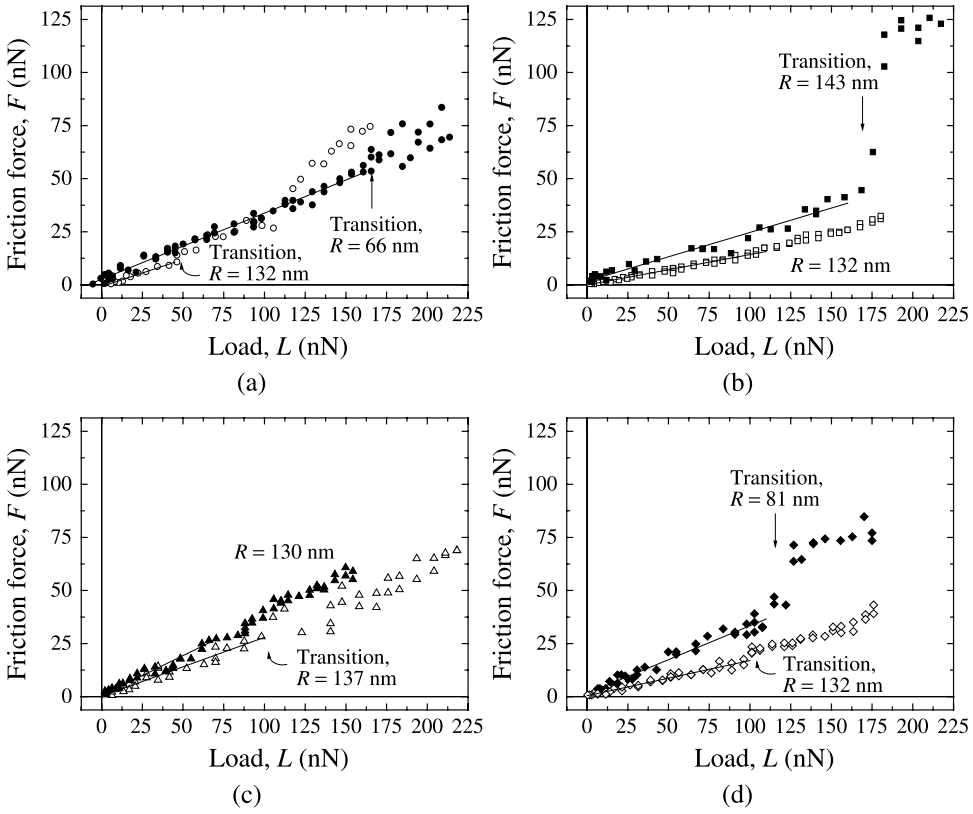

Figure 2. Friction force, F, as a function of applied load, L, measured in ethanol. Open symbols represent data obtained by scanning a monolayer-functionalized flat gold surface with a bare Si tip. Data obtained with monolayer-functionalized gold-covered tips are shown as filled symbols. (a) $n = 13$, $R_{Si} = 132$ nm, $R_{Au} = 66$ nm. (b) $n = 14$, $R_{Si} = 132$ nm, $R_{Au} = 143$ nm. (c) $n = 15$, $R_{Si} = 137$ nm, $R_{Au} = 130$ nm. (d) $n = 16$, $R_{Si} = 132$ nm, $R_{Au} = 81$ nm. The coefficients of friction μ obtained from linear fits to the low-load data are given in Table 1 and Fig. 3.

deformations at low loads will occur in the monolayer. At increased loads, the effective stiffness of such a layered system is still affected by the presence of the monolayer, and the analysis is more complicated than assumed in contact mechanics models for homogeneous elastic bodies, such as the Johnson–Kendall–Roberts (JKR) model [42], the Derjaguin–Muller–Toporov (DMT) model [43], or extensions of these [44]. Furthermore, in nanoscopic contacts, the pressure distribution should be affected by the atomic level structure of the substrate [45]. It is not yet established how well macroscopic models apply, although it has been shown that the influence of the substrate structure is reduced when a molecularly thin film is present in the contact [46].

In this work, we use the extended Thin-Coating Contact Mechanics (TCCM) model for the relationship between contact area and load. The details of this model [28, 29] and examples of its application to monolayer systems are shown elsewhere

[16, 47, 48], and only selected information needed for the discussion of the present work is shown here. In this model, the probe (spherical indenter) and the flat substrate are assumed to be rigid, which is a reasonable approximation at low load in our systems, since the Young's modulus of self-assembled monolayers is expected to be only a few GPa (cf. Discussion), but 78.5 GPa for gold [49], 70–80 GPa for SiO_2 [50], and 170 GPa for Si [38, 39].

The *F vs. L* data in our adhesive systems (Fig. 4) were compared to $F = S_c A$, where S_c is a constant, the critical shear stress, and A is the contact area at a given load L. The relationship between L, the radius of the contact area, a, and the work of adhesion ($W = 2\gamma$) in the extended TCCM model is given in non-dimensional form by [29]

$$\overline{L} = \frac{\pi}{4}\bar{a}^4 - \zeta^{1/2}\pi\bar{a}^2(2\overline{W})^{1/2} - 2\pi\overline{W}(1-\zeta), \tag{3}$$

where $\overline{L} = L/(E_u Rh)$, $\bar{a} = a/(\sqrt{Rh})$, and $\overline{W} = W/(E_u h)$. The uniaxial strain modulus is $E_u = E(1-\nu)/[(1+\nu)(1-2\nu)]$, where E is Young's modulus (in this case, 0.5 GPa, see Discussion) and ν is Poisson's ratio (0.4). The film thickness, h, is the thickness of one monolayer, $h = T$, in the case of a bare Si tip scanning a monolayer on the flat substrate, or two monolayers in contact, $h = 2T$, in experiments with monolayer-functionalized tips (cf. Tables 1 and 2). $\zeta = 2Wh/E_u\delta_c^2$ is a transition parameter ($0 \leqslant \zeta \leqslant 1$), a measure of the ratio of elastic deformation to the effective range of the surface forces. $\zeta = 0$ and $\zeta = 1$ correspond to limits where the range of adhesion is large and small compared to the elastic deformations (i.e., the DMT and JKR-like limits, respectively). The critical separation, δ_c, was assumed [29] to be 1 nm, as in a previous application of this model to monolayer systems [16].

In these experiments, the uncertainty in S_c mainly arises from propagation of the uncertainties in R, h, E_u, and W in the calculation of A [16]. The uncertainty in S_c can be calculated by differentiating equation (3) and using $\Delta R = 3$ nm ($R < 100$ nm) or 5 nm ($R \geqslant 100$ nm), $\Delta h = 0.1$ nm (monolayer on only the flat gold substrate, $h = T$) or 0.2 nm (monolayers on both surfaces, $h = 2T$), $\Delta E_u = 0.2$ GPa (ca. 20%), and $\Delta W = 0.002$ J/m^2. Following the procedure described in Ref. [16], we estimate that the relative uncertainty in S_c in the current experiments is 20%. Similarly, by differentiating the equation for ζ, its uncertainty is found to be 20%.

3. Results

3.1. Friction in Ethanol

The friction force F between monolayers on flat substrates and bare Si tips or monolayer-functionalized gold-covered tips was measured in ethanol. Representative results are shown as a function of load, L, in Fig. 2. In all systems, F increased linearly with L until a transition or plateau regime was reached, after which F was more scattered and also less reproducible from experiment to experiment. The on-

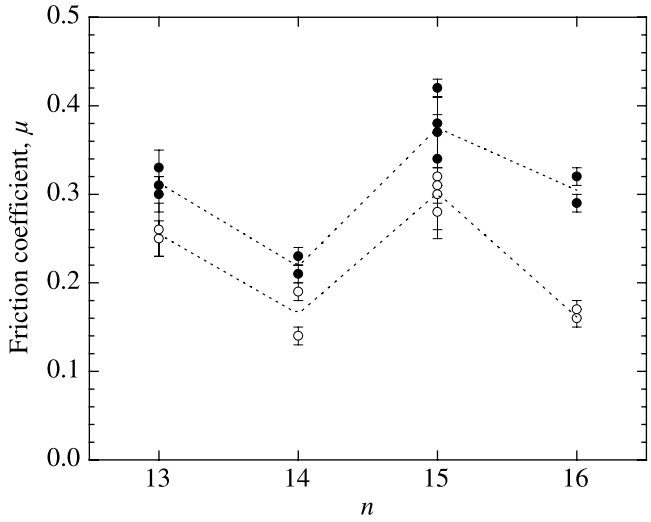

Figure 3. Coefficients of friction measured in ethanol for different n (cf. Fig. 2). Open and filled symbols indicate values obtained with bare Si tips and monolayer-functionalized tips, respectively. The error bars are the standard deviations from linear fits like those in Fig. 2. The dotted lines are drawn as guides.

set of this transition or plateau, which will be discussed in detail below, is indicated with an arrow in the cases where it could be clearly identified. In our analysis, we focus on the reproducible friction at low loads, below the transition. Experiments in addition to the ones in Fig. 2 were performed with tips having different radii and on monolayers prepared under identical conditions but on different occasions. The coefficients of friction μ obtained from linear fits ($F = \mu L$) to the low-load data in all these experiments are given in Table 1 and Fig. 3. The coefficients of friction were found to vary with the number of methylene units in the alkane chain, n, as shown in Fig. 3, and were independent of the tip radius, R, in the cases where tips with different R were used. The values of μ were significantly lower than those of simple aromatic and polyaromatic monolayers (thiophenol, $\mu = 1.2$–1.4; phenylthiophenol, $\mu = 0.9$–1.1 and terphenylthiol, $\mu = 0.6$) [16], but higher than those of a close-packed CH_3-terminated alkanethiol monolayer under similar conditions ($\mu = 0.02$–0.1, cf. Ref. [5], and discussion in Refs [14] and [15]). The coefficient of friction, μ, was higher with the monolayer-covered tips, which is different from what is observed for CH_3-terminated monolayers, where two confined monolayers generally give lower friction [1]. Our experiments in N_2 (see below) gave the expected result: higher S_c with a monolayer on only the flat surface, probed by a bare Si tip. Measurements of the friction of octadecanethiol SAMs in ethanol and N_2 (not shown) indicate that in that system, μ and S_c are higher when measured with a bare Si tip than with a monolayer-covered tip. As a whole, these observations are consistent with a model in which the enhanced friction for the monolayer-covered tips compared to that of the bare Si tips arises from attractive interfilm π–π interactions across the interface.

3.2. Friction in Dry N_2 Gas

Measurements of friction were also conducted under dry conditions (r.h. $\leqslant 0.7\%$), with the sliding contact immersed in dry N_2 gas. Figure 4 shows experimental data obtained with bare Si tips and monolayer-functionalized gold-covered tips. In several cases, the same tips were used as in the experiments in ethanol. No tip wear or monolayer damage was observed (cf. Discussion). In the experiments in N_2, where the adhesion was larger than in ethanol (the pull-off forces were larger, cf. Fig. 4, as expected from higher F_{vdw}/R, cf. Materials and Methods), F was not a linear function of L at the lowest loads. At higher loads, we observed transition regimes as

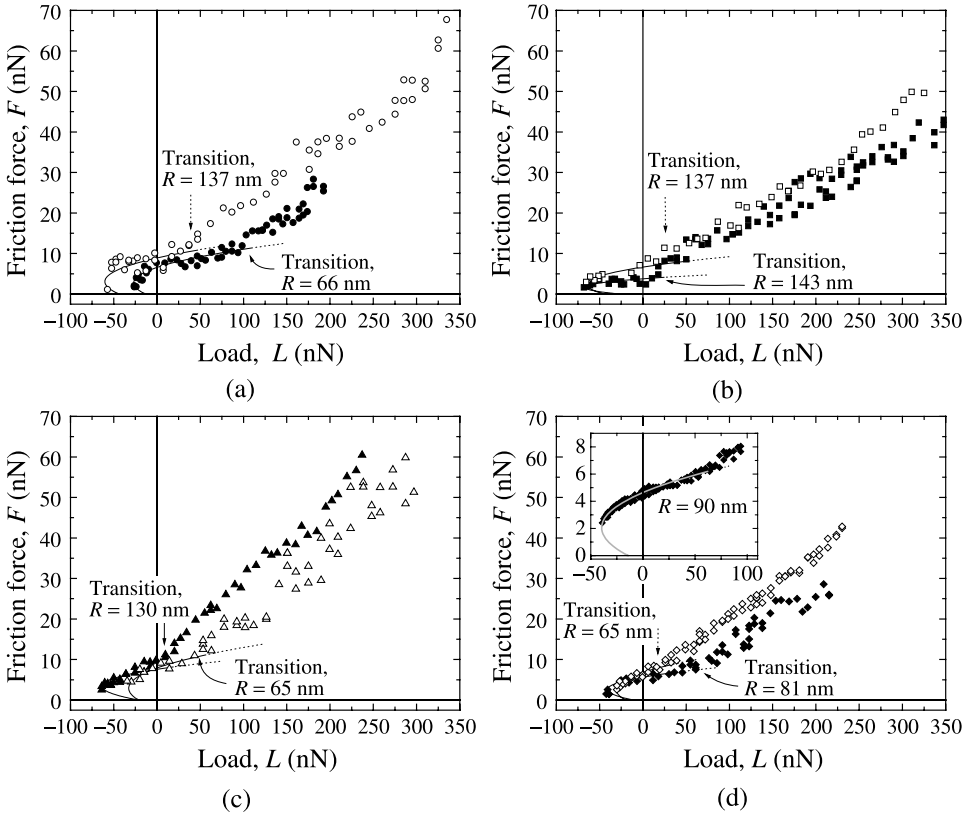

Figure 4. Friction force F *vs.* applied load L, measured in dry N_2 gas. Open symbols show data obtained using bare Si tips, and filled symbols show measurements with monolayer-functionalized gold-covered tips. (a) $n = 13, R_{\mathrm{Si}} = 137$ nm, $R_{\mathrm{Au}} = 66$ nm. (b) $n = 14, R_{\mathrm{Si}} = 137$ nm, $R_{\mathrm{Au}} = 143$ nm. (c) $n = 15, R_{\mathrm{Si}} = 65$ nm, $R_{\mathrm{Au}} = 130$ nm. (d) $n = 16, R_{\mathrm{Si}} = 65$ nm, $R_{\mathrm{Au}} = 81$ nm. Insert in panel (d): $n = 16$, monolayer on tip with $R_{\mathrm{Au}} = 90$ nm, where L was maintained below the threshold for the monolayer transition. The solid curves represent $S_{\mathrm{c}}A$, where the contact area A was calculated using the extended TCCM model with $E = 0.5$ GPa and $\nu = 0.4$. The curves are intended as comparisons to the low-load data only, below the transition regime. The values of S_{c} are provided in Table 2 and Fig. 5.

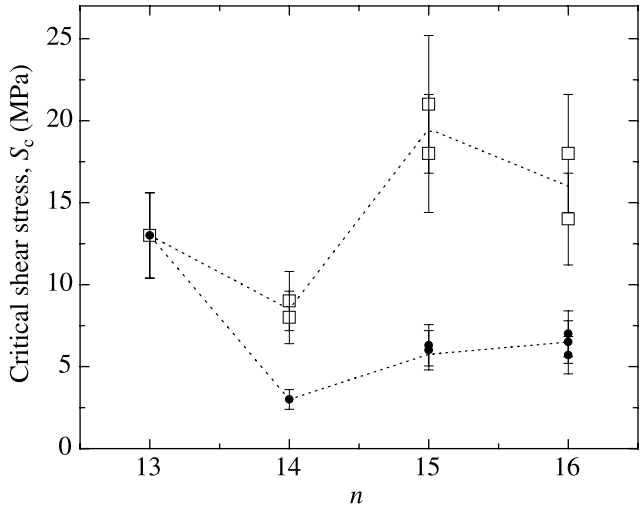

Figure 5. Critical shear stresses S_c obtained in dry N_2 gas for different n (cf. Fig. 4). Open and filled symbols show values obtained with bare Si tips and monolayer-functionalized tips, respectively. The error bars indicate a relative uncertainty of 20% (see text). The dotted lines are drawn as guides.

in the ethanol experiments, and above this regime F was again more scattered, less reproducible, and its functional form varied from experiment to experiment. The reproducible, non-linear data at low L are generally interpreted as area-dependent friction, since it is observed to depend on R.

The solid curves in Fig. 4 are $F = S_c A$, where $A = \pi a^2$ as a function of L was calculated using the extended TCCM model (equation (3)) with the parameters given in Table 2 and $E = 0.5$ GPa ($E_u = 1.1$ GPa). In the TCCM calculation, $h = T$ in the case of a single monolayer in contact with a bare Si tip and $h = 2T$ for two contacting monolayers. It should be noted that in cases where similar F values were measured with a bare Si tip and a monolayer-covered tip (cf. Fig. 4(b) and 4(d)), a larger S_c is, as expected, obtained for the single monolayer (Si tip), since the contact area in such a system is smaller (for given L, R and W). In Fig. 5, S_c is seen to vary with n for $n = 13$–15, whereas the result for $n = 16$ was similar to that of $n = 15$. In each system, the interfacial energy γ_{TCCM} ($=W/2$, $\Delta W = 0.002$ J/m^2) in Table 2 was in good agreement with γ_{vdW} calculated from bulk dielectric properties. The value of γ_{TCCM} for monolayer–monolayer contact (Table 2) can also be compared to the value of γ_{YD} from the contact angle measurements (Table 1), where a good agreement is found.

4. Discussion

In the following paragraphs, we discuss various aspects of the experimental data and details of the data analysis used to extract surface and interfacial energies and parameters describing the friction in different systems. The results are contrasted with those obtained in previous experiments on alkanethiols [9, 51–54] and poly-

Table 2.
Tip radii (R), critical shear stresses (S_c) at $E = 0.5$ GPa, transition parameter (ζ), and interfacial energy (γ_{TCCM}) measured in dry N_2

n	Bare Si tip ($h = T$)				SAM-covered tip ($h = 2T$)			
	R (nm)	S_c (MPa)[a]	ζ[a]	γ_{TCCM} (mJ/m^2)[b]	R (nm)	S_c (MPa)[a]	ζ[a]	γ_{TCCM} (mJ/m^2)[b]
13	137	13	0.27	35	66	13	0.50	32
14	137	8.0	0.29	35	143	3.0	0.61	38
	137	9.0	0.31	38				
15	65	21	0.34	40	130	6.3	0.66	39
	65	18	0.34	40	130	6.0	0.59	35
16	65	18	0.34	38	90	5.7	0.64	35
	65	14	0.34	38	81	7.0	0.73	40
					200	6.5	0.69	38

[a] Uncertainty 20%.
[b] $\Delta\gamma_{TCCM} = 1$ mJ/m^2.

aromatic thiol [16] self-assembled monolayers having different packing densities and rigidities.

4.1. Contact Angles and Interfacial Energy

The advancing contact angle of water (Table 1) showed no dependence on n, which was consistent with a previous study where slight differences were seen only with contacting liquids that were less polar than water [21]. The contact angles observed here were lower than those on monolayers derived from methyl-terminated alkanethiols, which is expected for the more polarizable phenyl groups, but higher than those on simple aromatic and polyaromatic thiols. Thiophenol, phenylthiolphenol and terphenyl thiol show advancing contact angles of 86–88°, and also have larger contact angle hysteresis with receding contact angles of 72–75° [16]. The values for the phenyl-terminated alkanethiols are consistent with their higher packing density (similar to the packing density of alkanethiols on gold) [21] compared to the abovementioned aromatic monolayers (where thiophenol, phenylthiolphenol and terphenyl thiol have molecular areas [16] of 0.4–0.7, 0.33 and 0.22 nm^2, respectively).

On close-packed aromatic structures (anthracene and naphthalene crystals), the highest contact angles of water, 94–95°, are found on crystal planes where the aromatic rings are oriented edge-on [55]. Our values are slightly lower, which is consistent with the structure in Fig. 1, where both odd and even n phenyl groups are oriented so that the face of the aromatic ring is, to some extent, available to the water. Systematic differences in contact angle observed with other contacting liquids [21] suggested that there was a slight difference in the exposure of the phenyl group for odd *vs.* even n.

The values of γ_{YD} (Table 1) are in good agreement with γ_{vdW} for the symmetric (monolayer-covered tip) system (32 mJ/m^2, cf. Materials and Methods), and with literature data on phenyldodecanethiol ($n = 12$), which showed that the monolayer surface energy was due purely to dispersion interactions with $\gamma^d = 34 \pm 2$ mJ/m^2 [31]. The data in Table 2 show that there is also a good agreement with the values of γ_{TCCM} ($=W/2$). Any differences in surface energy for odd and even values of n were too small to be detected with these methods and are thus probably not responsible for the differences in friction. In particular, it is unlikely that small differences in interfacial energy give rise to the distinct dependence on n of the friction in ethanol, where the adhesion was intentionally reduced. Instead, the odd–even effect on the friction might arise from the different orientations of the phenyl groups at the surface (shown schematically in Fig. 1), which will be discussed in detail below.

4.2. Monolayer Transition

In most of the data in Figs 2 and 4, a plateau, dip, or step in the *F vs. L* data was observed at high load (marked with an arrow in the figures). Similar transition regimes, ascribed to a reversible displacement of the molecules, have been observed for *n*-alkanethiol monolayers at pressures around 1 GPa [51]. They have also been seen for aromatic thiols and silanes [8, 14–16], and physisorbed fatty acids [23]. For a given monolayer, they occur at similar pressures in adhesive and non-adhesive contacts [15, 23]. The transition is reversible, i.e., as the load is decreased, the lower load regime is recovered. The data above the transition are typically more scattered and their functional form typically varies from experiment to experiment, which was not the case for the low-load data. The friction above the transition was not identical to that of pure gold (not shown), suggesting that the thiol molecules remained in the contact. In the current systems, the onset of the plateau was often gradual, making an accurate determination of a transition pressure difficult, but it was around 1 GPa as in the abovementioned systems. In a few cases, the data did not show a clear plateau (open symbols in Fig. 2(b), and filled symbols in Fig. 2(c), where the fit was limited to pressures below ca. 1 GPa), or the critical pressure was not reached (insert in Fig. 4(d)).

4.3. Friction in Non-adhesive and Adhesive Contacts

The frictional responses in ethanol and dry N_2 were clearly different. In ethanol (Fig. 2), we observed a linear dependence on L, with F approaching zero as L was reduced to zero, and with no dependence on R in the cases where several radii were investigated ($n = 13$ and 16, Table 1). The pull-off forces measured in normal force *vs.* separation curves (not shown) were no more than a few nN, which corresponds to an interfacial energy slightly lower than the calculated value of γ_{vdW} in ethanol (2–3 mJ/m^2, cf. Materials and Methods), but somewhat higher than the force expected at a separation of the average cross-sectional diameter [56] of an ethanol molecule ($D = 0.44$ nm). This observation, which also has been made for polyaromatic SAMs [16], suggests that at the closest separation, a full monolayer

of ethanol is not present between the tip and the sample. No layering of the ethanol was observed in the force *vs.* distance curves, which is consistent with the known reduction or absence of layering of solvents between amorphous or slightly rough monolayers [22]. The negative load of only a few nN at pull-off was not always discernible in the F *vs.* L data, since the surfaces tended to separate during scanning at the very lowest load so that no friction data could be obtained. This type of frictional response is commonly interpreted as load-dependent, and similar behavior has been observed in other systems: A linear trend in friction has been observed in single-asperity contact between mica surfaces due to repulsive hydration forces in aqueous electrolyte solution [57] and in self-assembled monolayer and polymer systems under conditions where the adhesion between these surfaces was low [8, 14–16, 22, 23, 26, 27].

In dry N_2, where the adhesion was higher, F was non-linear and depended on R (in the cases where tips with different R were used), which is commonly interpreted as an area-dependence. The stronger adhesion of the surfaces across N_2 arises from the stronger van der Waals attraction across N_2 gas than across ethanol, as shown by the calculation of γ_{vdW} in Materials and Methods. To evaluate the adhesion in terms of pull-off forces (as done above for the case of ethanol), we can consider the lowest load value in each data set in Fig. 4. For a given R, the pull-off forces agree well with those expected based on the calculated van der Waals interactions, which are 10–15 times stronger in N_2 than in ethanol. The different results in ethanol and N_2 do not arise from tip or monolayer damage since the different frictional responses (linear *vs.* non-linear) can be obtained with the same tip when switching from one environment (ethanol *vs.* N_2) and back. A non-linear increase in F with increasing L has been observed previously for adhering, unfunctionalized surfaces [22, 25, 58], and for adhering, self-assembled monolayers [16, 22, 23].

Many models for the dependence of the friction force on load and on contact area have been suggested based on empirical observations. It has been proposed that a dilation of the surfaces is necessary for sliding to occur, and that the external load and the adhesion forces contribute separately to the friction in such systems [22, 57]. In the absence of adhesion, the surfaces need to separate only against the external load (with no influence from the size of the contact area), whereas in adhesive systems there is an additional contribution from the interfacial energy (which acts over the real contact area). Depending on the strength of adhesion and the load regime, one of these contributions might dominate over the other. This situation is commonly expressed as $F = \mu L + S_c A$ (where A is a sublinear function of L) [22]. In one very simple model, the adhesion (interfacial energy) is incorporated into S_c only, which implies that if the interfacial energy were reduced, the second term would be strongly reduced or vanish, and only the linear load term ($F = \mu L$) would remain. In such cases, the friction would not depend on R, and data with different probe sizes could be directly compared with one another. The data in Fig. 2 (cf. values of μ in Table 1) are consistent with this model, which has been demonstrated in other systems with probe sizes differing by 5–6 orders of magnitude [8]. Other

models suggest that the friction force always depends on the contact area, and that a linear dependence on L arises from a non-constant (pressure-dependent) shear stress. Changes in the shear stress with pressure are certainly possible, especially considering the monolayer transition observed at higher loads. However, the linear F *vs.* L behavior has been observed in a wide variety of non-adhesive systems over wide ranges of loads and pressures, and it is unlikely that all of these systems can be rationalized by a pressure-dependent shear stress. In our adhesive systems, S_c appeared to be constant in the investigated range of loads (see Table 2), which has also been observed in other systems [16].

Differences between adhesive and non-adhesive systems have also been demonstrated in computer simulations, although not as two separate, additive terms. A linear dependence of F on L has been seen in molecular dynamics simulations of lubricated contacts (n-hexadecane between slightly rough gold surfaces), with a different slope and a shift along the L axis toward lower L as adhesion was introduced [24]. Recent molecular dynamics simulations of dry (unlubricated) contacts with atomic scale roughness showed sublinear and linear F *vs.* L-curves with and without adhesion, respectively [25].

We observed systematic differences in the friction with one *versus* two monolayers confined in the contact (i.e., with bare Si tips *vs.* monolayer-functionalized tips). In N_2, the systems with one monolayer showed a higher S_c (i.e., a higher friction), which might be expected if the presence of a monolayer on only one of the surfaces leads to a less well lubricated contact than when there is a monolayer on both surfaces. However, the opposite trend was observed in μ obtained from the measurements in ethanol. This different response in ethanol does not appear to arise from a contact area dependence, since the same proportionality between μ from experiments using bare or functionalized tips was observed irrespective of whether the radius of the monolayer-covered tip was smaller, larger, or approximately equal to the radius of the bare Si tip (cf. Table 2).

4.4. Monolayer Modulus

In experiments on polyaromatic thiol monolayers [16], the friction data in adhesive contact in N_2 could only be replicated (as $F = S_c A$) with areas from the extended TCCM model if a high Young's modulus was chosen, $E \geqslant 7$ GPa, ($\nu = 0.4$, $\zeta = 0.01$–0.02). Similar data on fatty acid monolayers required a much lower modulus, $E \leqslant 0.7$ GPa ($\nu = 0.4$, $\zeta > 0.1$) [16]. Moduli chosen outside these ranges gave curves with a rise too high or low compared with the experimental data, or did not reproduce the pull-off region (data at lowest L) well. Following a similar approach, the current data (Fig. 4) were best approximated with a Young's modulus in a narrow range of $E = 0.5 \pm 0.1$ GPa ($E_u = 1.1 \pm 0.2$ GPa).

A wide range of monolayer moduli can be found in the literature. Experiments using AFM to measure local compliance have suggested Young's moduli of $E = 0.2$–0.4 GPa for close-packed Langmuir–Blodgett fatty acid monolayers [59], and measurements of thickness changes during compression gave 1–5 GPa [60].

AFM experiments on the viscoelastic properties of close-packed alkanethiol monolayers have suggested a Young's modulus of 2 GPa [61]. Computer simulations of alkanethiol monolayers have indicated moduli around 20 GPa [62] and 36 GPa [49, 63], possibly representing ideal systems with few defects. A uniaxial strain modulus of $E_u = 3$ GPa ($E \approx 1.4$ GPa) has been found in molecular dynamics simulations of an alkylsilane monolayer compressed by a flat plate [64] and used successfully to compare calculated contact areas to molecular dynamics simulations of the contact between an AFM tip and the alkylsilane monolayer [48].

A Young's modulus of $E = 0.5$ GPa in our systems is quite similar to the experimental values reported for fatty acids, alkanethiols and alkylsilanes [16, 59–61], but differs clearly from the values for polyaromatic monolayers without methylene groups. These observations suggest that the deformations in the current, phenyl-terminated alkanethiol monolayers occur mainly in the alkane portion of the films. Furthermore, the overall lower friction compared to simple aromatic and polyaromatic thiol monolayers [14–16] is likely due not only to the higher packing in the current systems, but also to the possibility of facile reorientation of the terminal groups that are attached to flexible alkane chains.

4.5. Odd–Even Effects on Friction

The number of methylene units in alkanethiol monolayers or in spacers between functional end-groups and substrates has been shown to affect a number of properties such as the orientation of the terminal methyl group, the advancing contact angle of water and other liquids [52, 65–67], and the nanoscopic friction [9, 21, 52–54, 68, 69]. Interesting odd–even effects on packing density and molecular orientation have also been seen in biphenylalkanethiol [70, 71] and terphenylalkanethiol monolayers [13, 72], but their friction has not been studied.

Experimental work on alkanethiol SAMs on gold has suggested a higher friction with an even number of methylene units [53, 54]. Molecular dynamics simulations [68] of monolayers consisting of close-packed, methyl-terminated alkane chains have shown that compression and sliding induced significant conformational changes in the uppermost part of monolayers where the terminal CH_3– group was initially oriented close to the surface normal. In monolayers obtained by adding a methylene unit to this alkane chain, so that the terminal group was oriented away from the surface normal, compression and sliding induced mainly a slightly larger tilt of the terminal CH_3– group, without extensive defect formation, and this system consistently showed lower friction [68].

A possible rationalization of the odd–even effect that we observe for μ in ethanol is consistent with the computer simulation. Specifically, for even n the phenyl groups are more tilted from the surface normal than for odd n; consequently, less defect formation and energy dissipation can plausibly occur for even n during compression and sliding.

5. Summary

We have studied the friction of a series of self-assembled, phenyl-terminated alkanethiol monolayers. The adhesion between the monolayer-covered flat sample and the AFM tip was controlled by immersing the contact in ethanol or in dry N_2 gas. In ethanol, we observed linear friction ($F = \mu L$) that showed no dependence on the tip radius, R. In dry N_2, where the adhesion was stronger, F depended on R. The apparent area-dependence of F in this case was analyzed by comparing the experimental data to $F = S_c A$, where A was the contact area calculated according to the extended TCCM model and S_c was the critical shear stress, which was a constant for each system within the experimental uncertainty. The functional form of the friction data was well described by areas calculated using a Young's modulus of $E = 0.5$ GPa, which is lower than the modulus needed to describe similar data obtained on polyaromatic thiol monolayers. A systematic dependence of the coefficient of friction μ in ethanol on the number of methylene units in the alkane chain was found, with higher values obtained for odd n, where the terminal phenyl group is oriented closer to the surface normal than in films with even n.

Acknowledgements

We thank S. Lee for helpful discussions, J. Mead for access to the contact angle goniometer, T. Petterson for software for analysis of AFM data, and J. Whitten for advice on gold evaporation. Acknowledgment is made to the Donors of the American Chemical Society Petroleum Research Fund for support of this research through Grant #45101-G5 (MR). This work was also supported through NSF CAREER Award #NSF-CMMI 0645065 and by start-up funding (MR) through the NSF-funded Center for High-Rate Nanomanufacturing (CHN) (Award #NSF-0425826). The Robert A. Welch Foundation (grant E-1320) provided generous support for the work at the University of Houston.

References

1. E. E. Flater, W. R. Ashurst and R. W. Carpick, *Langmuir* **23**, 9242 (2007).
2. P. T. Mikulski and J. A. Harrison, *J. Am. Chem. Soc*. **123**, 6873 (2001).
3. M. Salmeron, *Tribology Lett*. **10**, 69 (2001).
4. S. Lee, Y.-S. Shon, R. Colorado Jr, R. L. Guenard, T. R. Lee and S. S. Perry, *Langmuir* **16**, 2220 (2000).
5. A. Lio, D. H. Charych and M. Salmeron, *J. Phys. Chem. B* **101**, 3800 (1997).
6. N. J. Brewer, B. D. Beake and G. J. Leggett, *Langmuir* **17**, 1970 (2001).
7. B. Bhushan and H. Liu, *Phys. Rev. B* **63**, 245412 (2001).
8. M. Ruths, N. A. Alcantar and J. N. Israelachvili, *J. Phys. Chem. B* **107**, 11149 (2003).
9. H. I. Kim and J. E. Houston, *J. Am. Chem. Soc.* **122**, 12045 (2000).
10. A. Ulman, *Acc. Chem. Res*. **34**, 855 (2001).
11. J. F. Kang, A. Ulman, S. Liao, R. Jordan, G. Yang and G.-y. Liu, *Langmuir* **17**, 95 (2001).
12. Y.-T. Tao, C.-C. Wu, J.-Y. Eu, W.-L. Lin, K.-C. Wu and C.-h. Chen, *Langmuir* **13**, 4018 (1977).

13. A. Shaporenko, M. Brunnbauer, A. Terfort, M. Grunze and M. Zharnikov, *J. Phys. Chem. B* **108**, 14462 (2004).
14. M. Ruths, *Langmuir* **19**, 6788 (2003).
15. M. Ruths, *J. Phys. Chem. B* **110**, 2209 (2006).
16. Y. Yang and M. Ruths, *Langmuir* **25**, 12151 (2009).
17. E. S. Forbes, *Wear* **15**, 87 (1970).
18. D. Wei and H. A. Spikes, *Wear* **111**, 217 (1986).
19. D. F. Heenan, K. R. Januszkiewicz and H. H. Sulek, *Wear* **123**, 257 (1988).
20. M. Nakano, T. Ishida, T. Numata, Y. Ando and S. Sasaki, *Jpn. J. Appl. Phys*. **43**, 4619 (2004).
21. S. Lee, A. Puck, M. Graupe, R. Colorado Jr, Y.-S. Shon, T. R. Lee and S. S. Perry, *Langmuir* **17**, 7364 (2001).
22. M. Ruths and J. N. Israelachvili, in: *Springer Handbook of Nanotechnology*, 2nd edn, B. Bhushan (Ed.), Chapter 30, pp. 859–924. Springer-Verlag, Berlin & Heidelberg (2007).
23. M. Ruths, S. Lundgren, K. Danerlöv and K. Persson, *Langmuir* **24**, 1509 (2008).
24. J. Gao, W. D. Luedtke, D. Gourdon, M. Ruths, J. N. Israelachvili and U. Landman, *J. Phys. Chem. B* **108**, 3410 (2004).
25. Y. Mo, K. T. Turner and I. Szlufarska, *Nature* **457**, 1116 (2009).
26. C. R. Hurley and G. J. Leggett, *Langmuir* **22**, 4179 (2006).
27. T. J. Colburn and G. J. Leggett, *Langmuir* **23**, 4959 (2009).
28. E. D. Reedy Jr, *J. Mater. Res*. **21**, 2660 (2006).
29. E. D. Reedy Jr, *J. Mater. Res*. **22**, 2617 (2007).
30. D. Valtakari, *MSc Thesis*, Department of Physical Chemistry, Åbo Akademi University, Åbo (Turku), Finland (2002).
31. F. Cavadas and M. R. Anderson, *J. Colloid Interface Sci.* **274**, 365 (2004).
32. J. N. Israelachvili, *Intermolecular and Surface Forces*. Academic Press, London (1991).
33. H. Y. Erbil, *Surface Chemistry of Solid and Liquid Interfaces*. Blackwell, Oxford (2006).
34. F. M. Fowkes, F. L. Riddle Jr, W. E. Pastore and A. A. Weber, *Colloids Surfaces* **43**, 367 (1990).
35. F. C. Whitmore, J. N. Cosby, W. S. Sloatman and D. G. Clarke, *J. Am. Chem. Soc*. **64**, 1801 (1942).
36. D. R. Lide (Ed.), *CRC Handbook of Chemistry and Physics*, 89th edn. CRC Press, Boca Raton, FL (2008–2009).
37. J. Visser, *Adv. Colloid Interface Sci*. **3**, 331 (1972).
38. Y. Liu, T. Wu and D. F. Evans, *Langmuir* **10**, 2241 (1994).
39. Y. Liu, D. F. Evans, Q. Song and D. W. Grainger, *Langmuir* **12**, 1235 (1996).
40. J. E. Sader, J. W. M. Chon and P. Mulvaney, *Rev. Sci. Instrum*. **70**, 3967 (1999).
41. C. P. Green, H. Lioe, J. P. Cleveland, R. Proksch, P. Mulvaney and J. E. Sader, *Rev. Sci. Instrum*. **75**, 1988 (2004).
42. K. L. Johnson, K. Kendall and A. D. Roberts, *Proc. R. Soc. London Ser. A* **324**, 301 (1971).
43. B. V. Derjaguin, V. M. Muller and Y. P. Toporov, *J. Colloid Interface Sci*. **53**, 314 (1975).
44. R. W. Carpick, D. F. Ogletree and M. Salmeron, *J. Colloid Interface Sci*. **211**, 395 (1999).
45. B. Luan and M. O. Robbins, *Nature* **435**, 929 (2005).
46. S. Cheng, B. Luan and M. O. Robbins*, Phys. Rev. E* **81**, 016102 (2010).
47. E. D. Reedy Jr, M. J. Starr, R. E. Jones, E. E. Flater and R. W. Carpick, in: *Proceedings of the 28th Annual Meeting of the Adhesion Society*, Mobile, AL, pp. 366–368 (2005).
48. M. Chandross, C. D. Lorenz, M. J. Stevens and G. S. Grest, *Langmuir* **24**, 1240 (2008).
49. A. Lio, C. Morant, D. F. Ogletree and M. Salmeron, *J. Phys. Chem. B* **101**, 4767 (1997).
50. R. G. Munro, *Elastic Moduli Data for Polycrystalline Oxide Ceramics*. NISTIR 6853, National Institute of Standards and Technology, Gaithersburg, MD (2002).

51. G.-y. Liu and M. Salmeron, *Langmuir* **10**, 367 (1994).
52. F. Tao and S. L. Bernasek, *Chem. Rev*. **107**, 1408 (2007).
53. S. S. Wong, H. Takano and M. D. Porter, *Anal. Chem*. **70**, 5209 (1998).
54. S. S. Perry, S. Lee, T. R. Lee, M. Graupe, A. Puck, R. Colorado Jr and I. Wenzl, *Polymer Preprints* **41**, 1456 (2000).
55. H. W. Fox, E. F. Hare and W. A. Zisman, *J. Colloid Sci.* **8**, 194 (1953).
56. S. Löning, C. Horst and U. Hoffmann, *Chem. Eng. Technol*. **24**, 242 (2001).
57. A. Berman, C. Drummond and J. Israelachvili, *Tribology Lett*. **4**, 95 (1998).
58. R. W. Carpick, N. Agrait, D. F. Ogletree and M. Salmeron, *Langmuir* **12**, 3334 (1996).
59. R. M. Overney, E. Meyer, J. Frommer, H.-J. Güntherodt, M. Fujihira, H. Takano and Y. Gotoh, *Langmuir* **10**, 1281 (1994).
60. V. V. Tsukruk, V. N. Bliznyuk, J. Hazel, D. Visser and M. P. Everson, *Langmuir* **12**, 4840 (1996).
61. M. Salmeron, G. Neubauer, A. Folch, M. Tomitori, D. F. Ogletree and P. Sautet, *Langmuir* **9**, 3600 (1993).
62. Y. Leng and S. Jiang, *J. Chem. Phys*. **113**, 8800 (2000).
63. R. Henda, M. Grunze and A. J. Pertsin, *Tribology Lett.* **5**, 191 (1998).
64. M. Chandross, personal communication (2008).
65. M. M. Walczak, C. Chung, S. M. Stole, C. A. Widrig and M. D. Porter, *J. Am. Chem. Soc*. **113**, 2370 (1991).
66. P. E. Laibinis, G. M. Whitesides, D. L. Allara, Y. T. Tao, A. N. Parikh and R. G. Nuzzo, *J. Am. Chem. Soc.* **113**, 7152 (1991).
67. N. Nishi, D. Hobara, M. Yakamoto and T. Kakiuchi, *J. Chem. Phys*. **118**, 1904 (2003).
68. P. T. Mikulski, L. A. Herman and J. A. Harrison, *Langmuir* **21**, 12197 (2005).
69. S. Lee, Y.-S. Shon, T. R. Lee and S. S. Perry, *Thin Solid Films* **358**, 152 (2000).
70. H.-T. Rong, S. Frey, Y.-J. Yang, M. Zharnikov, M. Buck, M. Wühn, Ch. Wöll and G. Helmchen, *Langmuir* **17**, 1582 (2001).
71. G. Heimel, L. Romaner, J.-L. Brédas and E. Zojer, *Langmuir* **24**, 474 (2008).
72. W. Azzam, A. Bashir, A. Terfort, T. Strunskus and Ch. Wöll, *Langmuir* **22**, 3647 (2006).